

# All-Pass Fractional OPF: A Solver-Friendly, Physics-Preserving Approximation of AC OPF

Milad Hasanzadeh, *Graduate Student Member, IEEE*, Amin Kargarian, *Senior Member, IEEE*, and Javad Lavaei, *Fellow, IEEE*

**Abstract**—This paper presents a fractional approximation of the AC optimal power flow (AC OPF) problem based on an all-pass approximation of the exponential power flow kernel. The classical AC OPF relies on trigonometric coupling between bus voltage phasors, which yields a nonconvex program with oscillatory derivatives that can slow, or in some cases destabilize, interior-point methods. We replace the trigonometric terms with an all-pass fractional (APF) approximation whose real and imaginary components act as smooth surrogates for the cosine and sine functions, and we introduce a pre-rotation to shift the argument of the approximation toward its most accurate region, ensuring that the reformulated power flow model preserves physical loss behavior, maintains the symmetry of the classical kernels, and improves the conditioning of the Jacobian and Hessian matrices. The proposed APF OPF formulation remains nonconvex, as in the classical model, but it eliminates trigonometric evaluations and empirically produces larger and more stable Newton steps under standard interior-point solvers. Numerical results on more than 25 IEEE and PGLib test systems ranging from 9 to 10,000 buses demonstrate that the APF OPF model achieves solutions with accuracy comparable to that of the classical formulation while reducing solver times, indicating a more solver-friendly nonconvex representation of AC OPF. All code, functions, verification scripts, and generated results are publicly available on GitHub, along with a README describing how to run and reproduce the experiments.

**Index Terms**—AC OPF, all-pass fractional OPF (APF OPF), nonlinear programming, IPM.

## NOMENCLATURE

### Sets

$\mathcal{N}$	Set of buses.
$\mathcal{G}$	Set of generators.
$\mathcal{G}_i$	Set of generators located at bus $i$ .
$\mathcal{L}$	Set of transmission lines.
<i>Parameters</i>	
$\mathbf{j}$	Imaginary unit, $\mathbf{j} := \sqrt{-1}$ .
$p_i^d, q_i^d$	Active/reactive load at bus $i$ .
$\underline{p}_i^g, \bar{p}_i^g$	Lower/upper active power generation limits.
$\underline{q}_i^g, \bar{q}_i^g$	Lower/upper reactive power generation limits.
$V_i, \bar{V}_i$	Lower/upper voltage magnitude limits.
$Y_{ij}$	Line admittance between buses $i$ and $j$ .
$ Y_{ij} $	Magnitude of admittance entry $Y_{ij}$ .
$\phi_{ij}$	Phase angle of admittance entry $Y_{ij}$ .
$\Delta\theta_{ij}, \bar{\Delta\theta}_{ij}$	Angle-difference limits.
$\bar{S}_{ij}$	Thermal rating of branch $(i, j)$ .
$f(p_i^g)$	Generation cost function.

This work was supported by the National Science Foundation under Grant ECCS-1944752 and Grant ECCS-2312086.

M. Hasanzadeh and A. Kargarian are with the Department of Electrical and Computer Engineering, Louisiana State University, Baton Rouge, LA 70803 USA (e-mail: mhasa42@lsu.edu; kargarian@lsu.edu).

J. Lavaei is with the Department of Industrial Engineering and Operations Research, University of California, Berkeley, CA 94720 USA (e-mail: lavaei@berkeley.edu).

$\theta_{\text{ref}}$	Reference (slack) bus angle.
$a$	All-pass design parameter.
$\theta_i^{dc}$	DC power flow voltage angle at bus $i$ .
$\delta_{ij}^{dc}$	DC angle difference on branch $(i, j)$ .
$\mu$	Barrier parameter for interior-point method.
$\alpha$	Step size in Newton/IPM updates.
<i>Variables</i>	
$p_i^g, q_i^g$	Active/reactive generation at bus $i$ .
$V_i$	Voltage magnitude at bus $i$ .
$\theta_i$	Voltage angle at bus $i$ .
$\delta_{ij}$	AC angle difference $\theta_i - \theta_j - \phi_{ij}$ .
$P_{ij}, Q_{ij}$	Power flow from bus $i$ to bus $j$ .
$P_{ji}, Q_{ji}$	Power flow from bus $j$ to bus $i$ .
$r(\delta)$	Complex all-pass kernel.
$r_{\cos}(\delta)$	Real part of $r(\delta)$ ; surrogate for $\cos(\delta)$ .
$r_{\sin}(\delta)$	Imaginary part of $r(\delta)$ ; surrogate for $\sin(\delta)$ .
$s$	Slack variables for inequality constraints.
$\lambda$	Lagrange multipliers for equality constraints.
$\nu$	Lagrange multipliers for inequality constraints.

## I. INTRODUCTION

THE AC optimal power flow (AC OPF) is a fundamental optimization problem in power system analysis, operation, and planning [1]. It aims to minimize total generation cost while satisfying the nonlinear AC power flow equations and operational constraints such as generator limits, voltage bounds, branch thermal limits, and phase-angle restrictions [2]. By explicitly modeling network physics through complex voltage phasors, AC OPF captures real and reactive power flows, losses, and voltage interactions via trigonometric coupling between voltage magnitudes and angles [3]. However, this nonlinear formulation leads to a highly nonconvex feasible set, making AC OPF computationally challenging, particularly for large-scale and heavily loaded transmission systems [2]–[5].

In general, research on AC OPF addresses its computational challenges through two main directions: relaxations and approximations [3]. Relaxation-based methods mitigate nonconvexity by reformulating or convexifying the original problem, often yielding optimization models that are easier to solve and may provide global or near-global optimality guarantees [6]–[9]. In contrast, approximation-based methods preserve the original OPF structure but simplify the AC power flow equations using linearized or reduced-complexity models, reducing computational effort at the expense of accuracy [10]–[12]. Although both approaches address nonlinear network physics, relaxations emphasize mathematical tractability and optimality bounds, whereas approximations prioritize physical interpretability and scalability for large-scale applications [3].

Relaxation-based approaches to AC OPF have been widely studied as a way to address the inherent nonconvexity of the problem. A major line of work focuses on convex relaxations,

where the nonlinear AC power flow equations are reformulated into convex optimization problems, such as semidefinite programming [13], second-order cone programming [2], [14], or quadratic convex [8] relaxations. These methods replace the original nonconvex feasible set with a convex superset, allowing global or near-global optimal solutions to be computed under certain conditions [2], [13]. When the relaxation is exact, the solution of the relaxed problem coincides with that of the original AC OPF, a phenomenon that has been demonstrated to occur for specific network topologies and operating regimes.

Approximation-based approaches to AC OPF reduce computational complexity by simplifying the nonlinear AC power flow equations. A classic example is the DC OPF model, which neglects reactive power, voltage magnitude variations, and losses, resulting in a linear and computationally efficient representation of network behavior [12]. To improve accuracy beyond DC OPF, various linearized and nonlinear approximations have been proposed, including Taylor-based expansions, fixed-point methods, and other reduced-complexity representations of trigonometric power flow relations [3]. More recent work has explored adaptive and data-driven approximation techniques that better capture nonlinear AC behavior across different operating conditions [10], [11]. In particular, fractional approximations based on Padé functions have been shown to achieve higher accuracy than DC OPF, and have been used to derive convex OPF formulations with improved fidelity [10]. Despite these advances, the accuracy of approximation-based methods generally depends on the operating point, and preserving consistency with physical power flow properties remains a key challenge [3].

From a computational perspective, the relevance of approximation choices becomes evident when considering how AC OPF problems are solved in practice. AC OPF is most commonly addressed using nonlinear programming solvers, among which interior-point methods (IPMs) have emerged as the dominant approach. IPMs solve constrained optimization problems by iteratively minimizing a sequence of barrier-augmented subproblems, where inequality constraints are incorporated into the objective through logarithmic barrier terms, and the resulting optimality conditions are solved using Newton-type steps [15], [16]. Due to their favorable scaling behavior and robustness for large nonlinear systems, IPMs are widely used in practical power system tools. In fact, the MATPOWER package adopts an IPM-based solver, MIPS, as its default and most reliable solver for AC OPF [17], [18].

Despite their effectiveness, the performance of IPMs is influenced by the smoothness and conditioning of the underlying model equations. In AC OPF, the trigonometric coupling between voltage magnitudes and phase angles produces highly nonlinear and oscillatory derivatives, which can result in ill-conditioned Jacobian and Hessian matrices, small Newton step sizes, and slow or unstable convergence, especially in large-scale or heavily loaded networks [3]. These challenges motivate the development of alternative AC OPF formulations that retain physical accuracy while offering smoother and more solver-friendly derivative structures. In particular, approximation models that align naturally with the numerical characteristics of IPMs provide a promising direction.

These observations motivate the use of fractional approximations not only as accuracy-enhancing tools, but also as a means of re-modeling the nonconvex AC power flow equations in a form that is more compatible with

Newton-based optimization algorithms. By reshaping the nonlinear trigonometric relationships into fractional functions, fractional models can improve derivative smoothness and conditioning, which is critical for robust IPM performance. Among fractional approximations, Padé approximations of complex exponential functions do not preserve unit magnitude and may introduce poles or near-singular behavior. When embedded within power flow equations, this will lead to artificial gain or attenuation, distorting the physical representation of power transfer and losses and potentially degrading numerical stability during optimization. These limitations highlight the need for fractional approximations that preserve both numerical robustness and fundamental physical properties of AC power flow models.

Motivated by the numerical challenges of solving AC OPF with interior-point methods and the limitations of classical polynomial approximations, this paper presents an all-pass fractional (APF) approximation of the AC power flow equations for OPF applications, termed APF OPF. The goal is not to eliminate the inherent nonconvexity of AC OPF, but to obtain a milder, more solver-friendly nonconvex representation by replacing the trigonometric sine and cosine terms with smooth APF functions. These APF functions preserve unit magnitude and the symmetry of the original power flow model, allowing the physical interpretation of power transfer and losses to be maintained. To improve approximation accuracy in practical operating regions, a pre-rotation of voltage angle differences based on a DC power flow solution is introduced, which centers the fractional approximation around typical angle values encountered during optimization. As a result, the APF OPF formulation retains the structure of the AC OPF model while exhibiting smoother and better-conditioned Jacobian and Hessian matrices that are suitable for interior-point solvers. Numerical experiments on more than 25 IEEE and PGLib test systems (9 to 10,000 buses) show that APF-OPF matches the accuracy of classical AC-OPF while reducing solver time, offering a more tractable nonconvex alternative in practice. All code and reproducible results are available at GitHub.

## II. AC OPF: MODELING AND INTERIOR-POINT METHODS

The standard AC OPF formulation is given in (1), where the decision variables are  $V$ ,  $\theta$ ,  $p^g$ , and  $q^g$ .

### A. AC OPF Model

$$\min_{\{V, \theta, p^g, q^g\}} \sum_{i \in \mathcal{G}} f(p_i^g) \quad (1a)$$

$$\text{s.t.} \quad \sum_{k \in \mathcal{G}_i} p_k^g - p_i^d = \sum_{j \in \mathcal{N}} V_i V_j |Y_{ij}| \cos(\delta_{ij}), \quad (1b)$$

$$\sum_{k \in \mathcal{G}_i} q_k^g - q_i^d = \sum_{j \in \mathcal{N}} V_i V_j |Y_{ij}| \sin(\delta_{ij}), \quad (1c)$$

$$\underline{p}_i^g \leq p_i^g \leq \bar{p}_i^g, \quad \underline{q}_i^g \leq q_i^g \leq \bar{q}_i^g, \quad (1d)$$

$$V_i \leq \bar{V}_i \leq \bar{V}_i, \quad (1e)$$

$$-\pi \leq \theta_i \leq \pi, \quad \theta_{\text{ref}} = 0, \quad (1f)$$

$$\underline{\Delta\theta}_{ij} \leq \theta_i - \theta_j \leq \bar{\Delta\theta}_{ij}, \quad \forall (i, j) \in \mathcal{L}, \quad (1g)$$

$$P_{ij}^2(V, \theta) + Q_{ij}^2(V, \theta) \leq \bar{S}_{ij}^2, \quad (1h)$$

$$P_{ji}^2(V, \theta) + Q_{ji}^2(V, \theta) \leq \bar{S}_{ij}^2. \quad (1i)$$

where  $\delta_{ij} := \theta_i - \theta_j - \phi_{ij}$ . The optimization problem (1) minimizes the total generation cost (1a). The active and reactive nodal balances (1b)–(1c) enforce Kirchhoff's laws using the trigonometric power flow kernel derived from the Y-bus. Generator limits are imposed by (1d), voltage bounds by (1e), and angular feasibility by (1f)–(1g). (1h)–(1i) enforce thermal limits on each transmission line.

The AC OPF problem is nonlinear because the power flow relations involve products of voltage magnitudes  $V_i V_j$  and nonlinear trigonometric functions  $\cos(\delta_{ij})$  and  $\sin(\delta_{ij})$ . The problem is also nonconvex. The cosine and sine terms create feasible regions that are not convex sets. This non-convexity is a fundamental challenge of AC OPF and is the reason why advanced solvers are used.

The AC power flow equations are symmetric with respect to phase-angle shifts: adding a constant to all  $\theta_i$  does not change any  $\delta_{ij}$  or any power flows. The underlying kernel also has unit magnitude, meaning

$$|\cos(\delta_{ij}) + \mathbf{j} \sin(\delta_{ij})| = 1.$$

Thus, the exponential kernel used in AC power flow does not introduce artificial losses—the model preserves the physical property that only network resistances contribute to real losses, preventing accumulation of spurious losses that would distort feasibility or optimality.

### B. Interior-Point Solution

Let  $x := \{V_i, \theta_i, p_i^g, q_i^g\}_{i \in \mathcal{N}}$  collect all decision variables. The power-balance constraints (1b)–(1c) form the nonlinear equality constraints, and generator, voltage, angle-difference, and thermal limits in (1d)–(1i) form the inequality constraints. Therefore, AC OPF can be written compactly as

$$\min_x f(x), \quad (2a)$$

$$\text{s.t. } h(x) = 0, \quad (2b)$$

$$g(x) \leq 0, \quad (2c)$$

where  $h(x)$  enforces active and reactive nodal balances, and  $g(x)$  aggregates all remaining operational limits. IPM solves (2) by replacing each inequality  $g_i(x) \leq 0$  with a logarithmic barrier term. For barrier parameter  $\mu > 0$ , the barrier-augmented objective becomes

$$\Phi(x, \mu) = f(x) - \mu \sum_i \ln(-g_i(x)), \quad (3)$$

so that the subproblem

$$\min_x \Phi(x, \mu) \quad \text{s.t. } h(x) = 0 \quad (4)$$

can be solved using Newton's method. To apply Newton's method, IPM forms the barrier Lagrangian

$$L(x, \lambda, \nu, \mu) = f(x) - \mu \sum_i \ln(-g_i(x)) + \lambda^T h(x) + \nu^T g(x), \quad (5)$$

where  $\lambda$  and  $\nu$  are multipliers for equality and (implicit) inequality constraints. The first-order optimality conditions are

$$\nabla_x L(x, \lambda, \nu, \mu) = 0, \quad (6a)$$

$$h(x) = 0, \quad (6b)$$

$$g(x) + s = 0, \quad (6c)$$

$$\nu_i s_i = \mu, \quad (6d)$$

where  $s$  denotes slack variables satisfying  $s > 0$  and  $\nu > 0$ . These relations encode primal feasibility, dual feasibility, and perturbed complementarity.

Because the active and reactive power-balance constraints involve trigonometric expressions, IPM needs analytic derivatives such as  $\frac{\partial P_i}{\partial V_k}$ , and  $\frac{\partial P_i}{\partial \theta_k}$ , obtained by differentiating the kernel

$$P_i = \sum_j V_i V_j |Y_{ij}| \cos(\delta_{ij}).$$

These derivatives populate the constraint Jacobians

$$J_h(x) = \nabla h(x)^T, \quad J_g(x) = \nabla g(x)^T, \quad (7)$$

and the Hessian of the barrier Lagrangian

$$H(x, \lambda, \nu, \mu) = \nabla_{xx}^2 L(x, \lambda, \nu, \mu). \quad (8)$$

At each IPM iteration, Newton's method linearizes the optimality system (6). Let  $r(x, \lambda, \nu, s, \mu)$  denote the concatenated primal, dual, and complementarity residuals. The Newton direction  $(\Delta x, \Delta \lambda, \Delta \nu, \Delta s)$  solves

$$K \begin{bmatrix} \Delta x \\ \Delta \lambda \\ \Delta \nu \\ \Delta s \end{bmatrix} = -r(x, \lambda, \nu, s, \mu), \quad (9)$$

where the KKT matrix is

$$K = \begin{bmatrix} H & J_h^T & J_g^T & 0 \\ J_h & 0 & 0 & 0 \\ J_g & 0 & 0 & I \\ 0 & 0 & S & N \end{bmatrix}, \quad (10)$$

with  $S = \text{diag}(s)$  and  $N = \text{diag}(\nu)$ . The structure of  $K$  reflects the entire AC OPF physics: the Jacobian captures the sensitivity of nodal balances and branch flows to voltage magnitudes and angles, while the Hessian captures curvature introduced by trigonometric coupling.

Once the Newton direction is computed, a step size is chosen to maintain  $s > 0$  and  $\nu > 0$ , and primal and dual variables are updated via

$$\begin{aligned} x^{(k+1)} &= x^{(k)} + \alpha \Delta x, & \lambda^{(k+1)} &= \lambda^{(k)} + \alpha \Delta \lambda, \\ \nu^{(k+1)} &= \nu^{(k)} + \alpha \Delta \nu, & s^{(k+1)} &= s^{(k)} + \alpha \Delta s. \end{aligned}$$

As  $\mu$  decreases, the iterates converge to a Karush–Kuhn–Tucker (KKT) point of AC OPF [19]. Interior-point performance, therefore, depends critically on the conditioning and smoothness of the Jacobians and Hessians derived from the AC power flow equations. Poorly conditioned derivatives—especially from the trigonometric kernel—can degrade Newton steps, slow convergence, or cause numerical instability, motivating the development of approximations with a more solver-friendly structure.

### III. PROPOSED APF OPF AND ITS PROPERTIES

We present the APF approximation of the trigonometric kernel of the power flow equations and discuss its properties in terms of (i) preserving the physical laws governing the electrical system and (ii) improving computational efficiency.

### A. All-Pass Kernel Approximation

The classical AC power flow model is built on the complex kernel

$$e^{j\delta} = \cos(\delta) + j \sin(\delta), \quad (11)$$

whose real and imaginary parts represent active and reactive coupling between bus voltage phasors. The magnitude of this kernel is exactly one, which ensures that only the network resistances contribute to real power losses. This unit-magnitude property is important because it prevents the artificial amplification or damping of voltage phasors as they propagate through the network.

To approximate the exponential kernel (11) in a fractional form, inspired by the concept of all-pass filters in signal processing [20], we use a first-order all-pass function

$$r(\delta) = \frac{1 + ja\delta}{1 - ja\delta}, \quad (12)$$

where  $a > 0$  is a design parameter controlling the shape of the approximation. The function  $r(\delta)$  is called all-pass because its magnitude is identically one for all real  $\delta$ . This can be verified by computing

$$|r(\delta)|^2 = \frac{(1 + ja\delta)(1 - ja\delta)}{(1 - ja\delta)(1 + ja\delta)} \quad (13)$$

$$= \frac{1 + (a\delta)^2}{1 + (a\delta)^2} = 1. \quad (14)$$

To relate (12) to trigonometric functions, we write its real and imaginary parts explicitly. Multiplying numerator and denominator by  $1 + ja\delta$  yields

$$r(\delta) = \frac{1 + ja\delta}{1 - ja\delta} = \frac{(1 + ja\delta)^2}{1 + (a\delta)^2}. \quad (15)$$

Expanding the numerator gives

$$(1 + ja\delta)^2 = 1 + 2ja\delta - (a\delta)^2, \quad (16)$$

so that

$$r(\delta) = \frac{1 - (a\delta)^2}{1 + (a\delta)^2} + j \frac{2a\delta}{1 + (a\delta)^2}. \quad (17)$$

This suggests the following approximations:

$$\cos(\delta) \approx r_{\cos}(\delta) := \frac{1 - (a\delta)^2}{1 + (a\delta)^2}, \quad (18)$$

$$\sin(\delta) \approx r_{\sin}(\delta) := \frac{2a\delta}{1 + (a\delta)^2}. \quad (19)$$

By choosing  $a$  appropriately, one can match the local slope of  $\sin(\delta)$  near the expansion point and obtain a good approximation in a neighborhood around that point. At the same time, the unit-magnitude property  $|r(\delta)| = 1$  guarantees that the fractional kernel preserves the loss behavior of the original exponential kernel.

### B. Pre-Rotation

The first-order all-pass functions in (18)–(19) approximate  $\sin(\delta)$  and  $\cos(\delta)$  best when their argument is close to zero. However, in a real power system, the electrical angle differences

$$\delta_{ij} = \theta_i - \theta_j - \phi_{ij}$$

are not necessarily small. They depend on loading conditions and the network structure, so directly applying the all-pass approximation to  $\delta_{ij}$  does not always give a good match.

To address this, we implement a pre-rotation step and shift the angle differences before applying the fractional approximation. We compute a DC power flow and/or DC OPF once, obtain the DC angles  $\theta_i^{dc}$ , and use them as a reference point. We are not using the DC solution as an initialization for AC OPF. Instead, we only use it to pre-rotate the angle differences so that the argument of the approximation is centered around zero.

From the DC solution, the corresponding angle difference on each line  $(i, j)$  is

$$\delta_{ij}^{dc} = \theta_i^{dc} - \theta_j^{dc} - \phi_{ij}. \quad (20)$$

We now write the AC angle difference as

$$\delta_{ij} = \delta_{ij}^{dc} + \Delta_{ij}, \quad (21)$$

where

$$\Delta_{ij} = (\theta_i - \theta_j) - (\theta_i^{dc} - \theta_j^{dc}). \quad (22)$$

The term  $\Delta_{ij}$  measures how far the current AC iterate is from the DC reference. In many practical cases, the DC angles are already close to the final AC angles. That means that, as the OPF solver converges,  $\Delta_{ij}$  tends to become small:

$$\Delta_{ij} \longrightarrow 0.$$

This observation is important because the APF is most accurate near zero. Using the decomposition in (21), we rewrite the trigonometric terms. If we define

$$\gamma_1 = \delta_{ij}^{dc}, \quad \gamma_2 = \Delta_{ij},$$

then  $\delta_{ij} = \gamma_1 + \gamma_2$ . Applying the angle-addition formulas step by step gives

$$\cos(\delta_{ij}) = \cos(\gamma_1 + \gamma_2) \quad (23)$$

$$= \cos(\gamma_1) \cos(\gamma_2) - \sin(\gamma_1) \sin(\gamma_2) \quad (24)$$

$$= \cos(\delta_{ij}^{dc}) \cos(\Delta_{ij}) - \sin(\delta_{ij}^{dc}) \sin(\Delta_{ij}), \quad (25)$$

and similarly

$$\sin(\delta_{ij}) = \sin(\delta_{ij}^{dc}) \cos(\Delta_{ij}) + \cos(\delta_{ij}^{dc}) \sin(\Delta_{ij}). \quad (26)$$

The key idea is that only the terms  $\cos(\Delta_{ij})$  and  $\sin(\Delta_{ij})$  depend on the AC variables. Since  $\Delta_{ij}$  stays small near the optimum, we can approximate them using the all-pass formulas introduced earlier:

$$\cos(\Delta_{ij}) \approx r_{\cos}(\Delta_{ij}) = \frac{1 - (a\Delta_{ij})^2}{1 + (a\Delta_{ij})^2}, \quad (27)$$

$$\sin(\Delta_{ij}) \approx r_{\sin}(\Delta_{ij}) = \frac{2a\Delta_{ij}}{1 + (a\Delta_{ij})^2}. \quad (28)$$

Substituting (27)–(28) into (25)–(26) gives the following approximations for each line:

$$\cos(\delta_{ij}) \approx \cos(\delta_{ij}^{dc}) r_{\cos}(\Delta_{ij}) - \sin(\delta_{ij}^{dc}) r_{\sin}(\Delta_{ij}), \quad (29)$$

$$\sin(\delta_{ij}) \approx \sin(\delta_{ij}^{dc}) r_{\cos}(\Delta_{ij}) + \cos(\delta_{ij}^{dc}) r_{\sin}(\Delta_{ij}). \quad (30)$$

To simplify notation, we define

$$\hat{r}_{\cos}(\delta_{ij}) := \cos(\delta_{ij}^{dc}) r_{\cos}(\Delta_{ij}) - \sin(\delta_{ij}^{dc}) r_{\sin}(\Delta_{ij}), \quad (31)$$

$$\hat{r}_{\sin}(\delta_{ij}) := \sin(\delta_{ij}^{dc}) r_{\cos}(\Delta_{ij}) + \cos(\delta_{ij}^{dc}) r_{\sin}(\Delta_{ij}), \quad (32)$$

so the AC power flow equations originally defined in (1b) and (1c) become APF power flow equations as

$$P_i^g - P_i^d = \sum_j V_i V_j |Y_{ij}| \hat{r}_{\cos}(\delta_{ij}), \quad (33)$$

$$Q_i^g - Q_i^d = \sum_j V_i V_j |Y_{ij}| \hat{r}_{\sin}(\delta_{ij}), \quad (34)$$

where the functions  $\hat{r}_{\cos}$  and  $\hat{r}_{\sin}$  depend only on the shifted angle difference  $\Delta_{ij}$  and the DC reference  $\delta_{ij}^{dc}$ . A similar substitution is made for the expressions defining  $P_{ij}$  and  $Q_{ij}$  in the thermal-limit constraints, so the entire APF OPF model becomes consistent.

### C. APF OPF Model

The resulting APF OPF is

$$\min_{\{V, \theta, p^g, q^g\}} \sum_{i \in \mathcal{G}} f(p_i^g) \quad (35a)$$

$$\text{s.t. } \sum_{k \in \mathcal{G}_i} p_k^g - p_i^d = \sum_{j \in \mathcal{N}} V_i V_j |Y_{ij}| \hat{r}_{\cos}(\delta_{ij}), \quad (35b)$$

$$\sum_{k \in \mathcal{G}_i} q_k^g - q_i^d = \sum_{j \in \mathcal{N}} V_i V_j |Y_{ij}| \hat{r}_{\sin}(\delta_{ij}), \quad (35c)$$

$$p_i^g \leq p_i^d \leq \bar{p}_i, \quad q_i^g \leq q_i^d \leq \bar{q}_i, \quad (35d)$$

$$\underline{V}_i \leq V_i \leq \bar{V}_i, \quad (35e)$$

$$-\pi \leq \theta_i \leq \pi, \quad \theta_{\text{ref}} = 0, \quad (35f)$$

$$\underline{\Delta\theta}_{ij} \leq \theta_i - \theta_j \leq \bar{\Delta\theta}_{ij}, \quad \forall (i, j) \in \mathcal{L}, \quad (35g)$$

$$P_{ij}^2(V, \theta; \text{APF}) + Q_{ij}^2(V, \theta; \text{APF}) \leq \bar{S}_{ij}^2, \quad (35h)$$

$$P_{ji}^2(V, \theta; \text{APF}) + Q_{ji}^2(V, \theta; \text{APF}) \leq \bar{S}_{ij}^2. \quad (35i)$$

In (35h)–(35i), the branch-flow expressions  $P_{ij}(\cdot; \text{APF})$  and  $Q_{ij}(\cdot; \text{APF})$  are computed using the same network model as in the AC OPF, except that every occurrence of  $\cos(\delta_{ij})$  and  $\sin(\delta_{ij})$  in the line-flow formulas is replaced by  $\hat{r}_{\cos}(\delta_{ij})$  and  $\hat{r}_{\sin}(\delta_{ij})$ , respectively, ensuring consistency between nodal balances and thermal-limit constraints.

### D. Properties of APF OPF Formulation

We analyze the main structural and numerical properties of the APF OPF formulation and explain why these properties lead to improved numerical behavior without altering the underlying physics of the power flow model.

**1) Unit-Magnitude Property and Preservation of Power Losses:** One of the most important properties of the all-pass function is that its magnitude is identically equal to one for all real angle differences:

$$|r(\delta)| = 1 \quad \text{for every real } \delta.$$

As a result, the APF approximation does not introduce any artificial attenuation or amplification of power flow terms. In particular, real power losses continue to arise solely from the physical resistances of transmission lines, exactly as in the classical AC OPF formulation. This ensures that the approximation does not distort the loss model or alter the physical interpretation of resistive dissipation.

**2) Symmetry Preservation of Trigonometric Structure:** Another key property of the all-pass approximation is that its real and imaginary components,

$$r_{\cos}(\delta) = \frac{1 - (a\delta)^2}{1 + (a\delta)^2}, \quad r_{\sin}(\delta) = \frac{2a\delta}{1 + (a\delta)^2},$$

preserve the symmetry of the trigonometric functions they replace. Evaluating these expressions at  $-\delta$  yields

$$r_{\cos}(-\delta) = r_{\cos}(\delta), \quad r_{\sin}(-\delta) = -r_{\sin}(\delta),$$

showing that  $r_{\cos}$  is an even function and  $r_{\sin}$  is an odd function. This mirrors the symmetry of  $\cos(\delta)$  and  $\sin(\delta)$ , respectively. Since AC power flow equations rely critically on how active and reactive power terms change sign when angle differences reverse direction, preserving this odd–even structure helps maintain the physical consistency of the model.

**3) Role of APF Parameter and Numerical Smoothness:** The parameter  $a$  controls the curvature of the all-pass functions as a function of the angle difference  $\delta$ . If  $a$  is chosen too large, the functions become steep and may introduce numerical difficulties. If  $a$  is chosen too small, the approximation becomes overly flat and loses accuracy. Importantly, the denominator of the all-pass function never vanishes for real  $\delta$ , so the model does not suffer from real-axis poles.

In practice, a moderate value such as  $a = 0.5$  provides a good balance between accuracy and numerical stability. With this choice, the APF remains smooth and well behaved over the range of angle differences typically encountered in AC OPF solutions, as confirmed by the numerical experiments reported later in the paper.

**4) Derivative Structure and Improved Conditioning:** Although the APF formulation remains nonlinear and nonconvex, its derivative structure differs from that of the classical trigonometric formulation. In the standard AC OPF model, the Jacobian and Hessian contain derivatives such as

$$\frac{d}{d\delta} \sin(\delta) = \cos(\delta), \quad \frac{d}{d\delta} \cos(\delta) = -\sin(\delta),$$

which oscillate as  $\delta$  varies. These oscillations cause frequent sign changes and rapid curvature variation, which can lead to poorly conditioned Newton steps in interior-point methods.

In contrast, the derivatives of the all-pass components,

$$\frac{d}{d\delta} r_{\cos}(\delta) = \frac{-4a^2\delta}{(1 + (a\delta)^2)^2}, \quad \frac{d}{d\delta} r_{\sin}(\delta) = \frac{2a(1 - (a\delta)^2)}{(1 + (a\delta)^2)^2},$$

are smooth fractional functions. They do not oscillate and exhibit gradual changes in curvature. As  $|\delta|$  increases, the denominator dominates and naturally damps the slope, leading to more stable and predictable Jacobian and Hessian matrices during optimization.

**5) Computational Efficiency of Fractional Evaluations:** From a computational standpoint, the APF formulation replaces trigonometric evaluations with simple arithmetic operations involving addition, multiplication, and division. Both the functions and their derivatives can be computed efficiently without calling expensive trigonometric routines. For large-scale OPF problems, this reduction in per-iteration computational cost becomes significant, contributing to faster solver runtimes.

### 6) Impact on Newton Steps and Solver Convergence:

Because the derivatives of the APF OPF constraints are smoother and their curvature varies more slowly, interior-point solvers are able to construct better-conditioned Newton steps. In practice, this leads to larger and more reliable steps during each iteration. Larger Newton steps reduce the number of iterations required to reach convergence, which explains the consistent reductions in IPOPT iterations and solver time observed in the numerical results.

This effect becomes particularly pronounced in large-scale networks, where oscillatory trigonometric behavior can otherwise cause unstable or overly conservative step sizes.

Overall, the APF OPF formulation preserves the essential physics of PF, including loss modeling, angle symmetry, and directional behavior, while offering a numerical structure that is more compatible with interior-point optimization methods. By combining physical fidelity with smoother derivatives and reduced computational overhead, the APF formulation provides an accurate yet more solver-friendly alternative to the classical trigonometric AC OPF model.

### E. APF vs. Classical Kernels

The functions  $r_{\sin}(\delta)$  and  $r_{\cos}(\delta)$  are plotted together with  $\sin(\delta)$  and  $\cos(\delta)$  over the interval  $[-180^\circ, 180^\circ]$ . These plots show the overall accuracy of the fractional approximation and indicate the angle regions where the curves match more closely.

Fig. 1a shows  $\sin(\delta)$  and  $r_{\sin}(\delta)$  without any pre-rotation. Fig. 1b shows the same comparison for the cosine function. In both cases, the all-pass functions follow the classical trigonometric curves well near the origin. Larger deviations appear when  $|\delta|$  becomes large, which is outside typical operating ranges. This observation is consistent with how the first-order fractional form is constructed, since it is centered at zero and provides its best accuracy near that point.

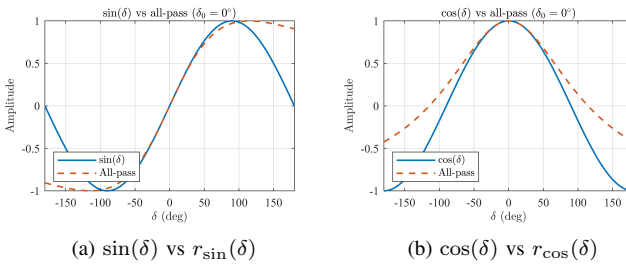


Fig. 1: Comparison of classical trigonometric kernels and their all-pass approximations over  $[-180^\circ, 180^\circ]$  with no pre-rotation

The derivatives of the functions are also compared because they directly affect the Jacobian and Hessian used by IPM. The corresponding derivatives of the fractional functions depend on smooth fractional expressions whose slopes decrease gradually as  $|\delta|$  increases. Fig. 2 shows the comparison of the classical and all-pass derivatives over the same angle interval. Near zero, the slopes match closely, while for large angles the fractional functions exhibit gentler behavior.

With the pre-rotation applied to the APF OPF approximation, the argument of the all-pass functions becomes  $\Delta_{ij}$ , which is close to zero for many lines. To show how shifting the argument affects the approximation, several plots with different shift values are provided in Fig. 3. In each case,  $r_{\sin}(\delta - \text{shift})$  and  $r_{\cos}(\delta - \text{shift})$  are compared with the corresponding

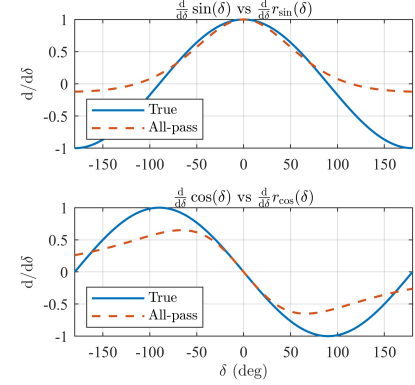


Fig. 2: Comparison of the rate of variation of the trigonometric functions and their all-pass approximations over  $[-180^\circ, 180^\circ]$  with no pre-rotation

trigonometric functions. The location where the curves align most closely moves horizontally with the shift. This illustrates how the shift places the high-accuracy window of the fractional functions near the actual operating angles of the network.

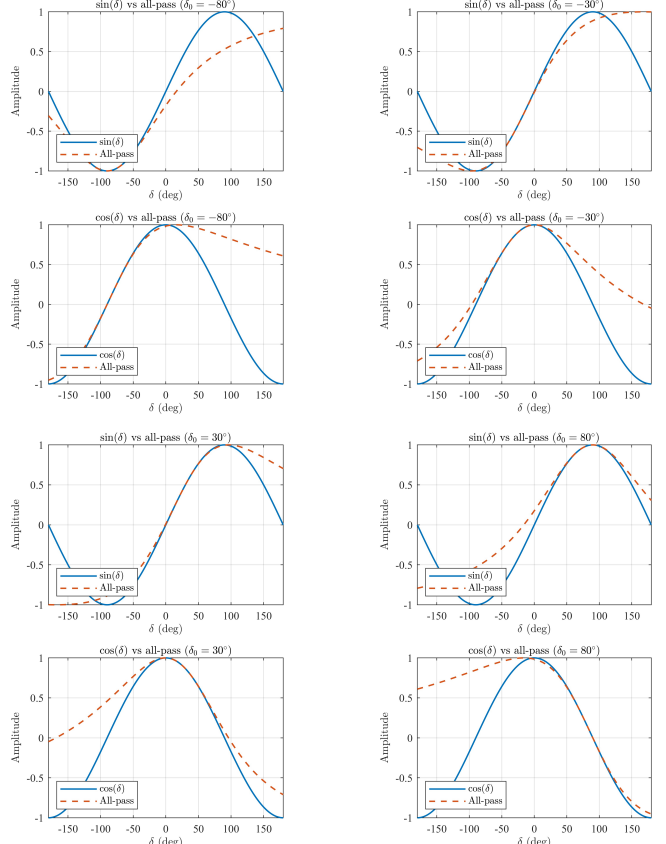


Fig. 3: Effect of applying different shifts to the argument of the all-pass kernels

These comparisons indicate that APF closely follows the classical trigonometric kernels in the operating region of OPF and that pre-rotation further improves the alignment by centering the approximation around expected angle differences.

## IV. NUMERICAL EXPERIMENTS AND RESULTS

We evaluate the numerical performance and solution quality of the proposed APF OPF formulation in (35) relative to the classical AC OPF model in (1). All simulations are

reproducible using the publicly available repository at GitHub, which includes the codebase, configuration files, and scripts for regenerating the reported figures and tables.

### A. Numerical Setup and Solvers

All simulations are carried out using IPOPT [15], which is an interior-point optimizer designed for large nonlinear problems. IPOPT solves a sequence of barrier subproblems and relies on Newton steps, so its performance is sensitive to the smoothness and well-conditioning of the model equations. This makes it an appropriate platform for evaluating whether replacing trigonometric terms with the APF kernel produces more stable numerical behavior.

The AC OPF (1) and APF OPF (35) are implemented in two different environments: YALMIP [21] and CasADi [22]. YALMIP provides a symbolic MATLAB interface that is easy to develop and debug, while CasADi builds a computational graph and generates efficient derivative code. For small and medium-sized networks, both work well, but CasADi generally scales better on large PGLib cases due to its optimized automatic differentiation and sparsity handling. In total, four solver functions are used:

- `acopf_exp` (YALMIP + IPOPT, AC OPF),
- `acopf_allpass` (YALMIP + IPOPT, APF OPF),
- `acopf_exp_ipopt_casadi` (CasADi + IPOPT, AC OPF),
- `acopf_allpass_ipopt_casadi` (CasADi + IPOPT, APF OPF).

All four functions accept the same core inputs: a MATPOWER case name, a percentage parameter  $m$  for optional scaling of line ratings (for manually making 90 percent of lines have reduced  $m$  percent line rates), and an optional IPOPT override structure. The APF versions accept an additional vector  $a_{\text{params}}$  for specifying the poles of the fractional kernel; if omitted, a single pole is chosen automatically from the network's angle band. Each function returns a result structure containing bus voltages, generator outputs, objective value, angle information, congestion, solver time, and (for the APF solvers) the pre-rotation time and the edge-angle differences.

To evaluate the accuracy, optimality, and physical feasibility of the proposed all-pass formulation, a dedicated comparison routine, `compare_acopf_results(res_exp, ok_exp, res_allpass, ok_allpass)`, is employed. This routine preserves both solver outputs intact and compares them in a standardized manner. Optimality is assessed via absolute and relative objective gaps between the AC OPF and APF OPF solutions. Angle behavior is analyzed directly from solver outputs using raw bus angle differences and kernel-level edge angle differences, for which maximum, average, and minimum values are reported.

In this context, feasibility refers to whether the APF OPF solution, when evaluated outside the optimization model, satisfies the original nonlinear AC power flow equations and all operational constraints. Specifically, the APF OPF voltage magnitudes, phase angles, and generator outputs are substituted into the exact trigonometric AC equations to recompute nodal active and reactive power injections and branch power flows. These recomputed quantities are then checked against power-balance equations, voltage magnitude bounds, generator active and reactive limits, branch thermal limits, and branch angle-difference limits. All feasibility checks are performed using a user-defined numerical tolerance, which accounts

for floating-point errors and solver termination accuracy; a constraint is considered satisfied if its violation does not exceed this tolerance. Feasibility is reported both as an overall pass/fail indicator and through detailed violation counts that identify the number and location of buses, generators, and branches violating each constraint class.

Congestion is evaluated using solver-reported binding constraints, and congested lines are compared between the AC OPF and APF OPF solutions using physical (undirected) line matching. Computational performance is also compared using elapsed solver times, allowing for a direct assessment of the efficiency of the APF OPF relative to the AC OPF model.

All experiments are executed through a main driver script, `run_acopf_compare(case_name, mode, m)`, where `mode` selects YALMIP or CasADi. The script automatically calls both AC OPF and APF OPF solvers, collects their results, runs the comparison function, and prints the numerical report. This creates a unified and repeatable numerical experiment pipeline for all IEEE and PGLib test cases used in the paper.

### B. Benchmark Results Across Network Sizes

The test set spans from small IEEE and MATPOWER networks to large-scale PGLib transmission systems with more than 10,000 buses. All experiments are conducted using identical solver configurations to isolate the impact of the kernel approximation from solver parameter tuning.

Table I reports unified performance and diagnostic metrics for all benchmark cases, including time speedup, optimality gap, feasibility under true AC re-evaluation, detailed counts of constraint violations, congestion consistency, and the maximum branch-wise voltage-angle difference  $\theta_i - \theta_j$ . For clarity, the results are discussed according to three size categories: small systems (9–300 buses), medium systems (588–3,375 buses), and large systems (4,601–10,480 buses).

We first clarify how the feasibility-related quantities reported in Table I are computed. Feasibility is evaluated by substituting the APF OPF solution into the original nonlinear AC power flow equations and operational constraints. In particular, bus active and reactive power balance mismatches are computed by replacing the APF OPF voltage magnitudes, phase angles, and generator outputs into the exact trigonometric AC power flow equations, and the resulting mismatches are explicitly evaluated and reported.

All remaining feasibility checks correspond to inequality constraints, including voltage magnitude limits, generator active and reactive power limits, branch thermal limits, and branch angle-difference limits. For these constraints, a marginal mismatch metric is reported. Specifically, a value of zero indicates that the constraint is satisfied for all elements, while any nonzero value represents the magnitude by which a constraint is violated. For each constraint class, Table I reports the number of elements whose violation exceeds a specified numerical tolerance, along with the maximum and average violation magnitudes across all elements. These columns therefore provide a direct assessment of whether the APF OPF solution is physically feasible when evaluated under the exact AC OPF constraints.

In addition to feasibility diagnostics, Table II reports variable mismatches between the AC OPF and APF OPF solutions. In this table, mismatches in generator dispatch, voltage magnitudes, voltage angles, and branch power flows are computed by directly comparing the outputs of the two

formulations. Only the maximum and average mismatch values are reported. This analysis is limited to medium- and large-scale systems, as mismatches in small-scale networks are consistently negligible and do not provide additional insight.

A few large-scale cases, such as `case8387_pegase`, exhibit feasibility or congestion mismatches. These cases correspond to networks where the classical AC OPF model itself converges only to acceptable-level solutions or approaches step-length failure, making both formulations sensitive to numerical conditioning. In all well-conditioned networks, the AC OPF and APF OPF formulations agree in feasibility outcomes, congestion patterns, and voltage-angle behavior.

Across all benchmark cases, three formulations are evaluated: the classical AC OPF, the APF OPF with DC power flow based pre-rotation, and the APF OPF with DC OPF based pre-rotation. Numerical experiments indicate that DC-OPF-based pre-rotation generally yields slightly more accurate solutions than DC-PF-based pre-rotation when compared against the classical AC OPF. Nevertheless, the solutions obtained using both pre-rotation strategies remain highly comparable to the AC OPF in terms of objective value, feasibility, congestion patterns, and voltage-angle behavior.

Despite its improved accuracy, DC-OPF-based pre-rotation often results in longer solver times compared to both the classical AC OPF and the APF OPF with DC-PF-based pre-rotation. In contrast, DC-PF-based pre-rotation consistently achieves faster solution times across all tested cases while maintaining solution accuracy that is nearly indistinguishable from the classical AC OPF. For this reason, DC-PF-based pre-rotation is adopted as the default configuration throughout the numerical study.

Accordingly, all results reported in Tables I and II are obtained using DC-PF-based pre-rotation, with the exception of `case118`, `case8387_pegase`, `case9591_goc`, and `case10480_goc`. In these cases, DC-OPF-based pre-rotation provides more accurate solutions while also yielding smaller solver times than DC-PF-based pre-rotation, and is therefore used in place of the default setting.

1) *Small Systems (9–300 Buses)*: This category includes standard IEEE and MATPOWER test cases ranging from `case9` to `case300`. These networks are relatively small and usually have mild nonlinear behavior, limited congestion, and well-conditioned operating points. All experiments for small-scale systems are performed using YALMIP modeling.

a) *Speedup*: For all small-scale systems, the APF formulation shows a clear reduction in computational time compared to the classical AC OPF. According to Table I, the time speedup varies from about 11% in `case30` to more than 70% in `case57`, with most cases achieving speedups between 20% and 45%. These improvements are obtained without changing solver tolerances or stopping criteria. Therefore, the speedup mainly comes from better numerical conditioning of the problem introduced by the APF kernel, rather than changes in solver settings.

b) *Optimality Gap*: For all small-scale test cases, the APF formulation produces objective values that are identical to those of the classical AC OPF within numerical precision. As shown in Table I, the optimality gap is zero for all systems in this group. This indicates that the APF kernel does not affect the optimal cost or the optimal operating point of the problem.

c) *Feasibility*: All APF solutions for small networks remain feasible when they are evaluated using the exact

nonlinear AC power flow equations and constraints. The active and reactive power balance mismatches at buses are very small and always below the specified tolerances. Voltage magnitude limits, generator active and reactive power limits, branch thermal limits, and angle difference constraints are all satisfied, with no violations reported in Table I. These results confirm that the APF solutions are physically consistent with the original AC OPF model for all small-scale cases.

d) *Congestion*: Most small-scale networks do not have congested transmission lines. In cases where congestion exists, such as `case30`, the APF formulation identifies exactly the same congested branches as the AC OPF solution. As shown by the zero congestion mismatch values in Table I, there is no difference between the two formulations in terms of congestion.

e) *Max  $\theta_i - \theta_j$* : The maximum branch-wise voltage angle differences remain within reasonable physical limits for all small-scale systems. For distribution-type networks, these angle differences are typically below 1°, while for more meshed transmission networks they are larger. The highest observed value is about 20.7° in `case300`. The close agreement between the AC OPF and APF OPF results shows that the APF kernel preserves the angle behavior of the original AC power flow model.

2) *Medium Systems (588–3375 Buses)*: The medium-scale category consists of more challenging PGLib transmission networks with denser meshed topology and stronger nonlinear coupling. This group includes `case588_sd5`, `case1354_pegase`, `case2383wp_k`, `case2746wp_k`, `case2869_pegase`, and `case3375wp_k`. All medium-scale experiments are conducted using the CasADI-based implementation.

a) *Speedup*: For medium-scale systems, the APF formulation consistently achieves noticeable reductions in computational time compared to the classical AC OPF. As reported in Table I, time speedup values range from approximately 20% to 50%, with most cases showing speedups between 27% and 40%. The largest improvements are observed in cases such as `case2383wp_k` and `case2869_pegase`. These results indicate that the APF kernel improves numerical conditioning of the nonlinear equations, leading to faster convergence without modifying solver settings.

b) *Optimality Gap*: Across all medium-scale networks, the optimality gap remains very small. As shown in Table I, gap values are either zero or below  $2 \times 10^{-3}\%$ . This confirms that the APF formulation preserves the objective value of the AC OPF even for larger and more nonlinear systems, and that the economic dispatch structure remains essentially unchanged.

c) *Feasibility*: Most medium-scale APF solutions remain feasible when evaluated under the exact nonlinear AC power flow equations. Bus active and reactive power balance mismatches are generally below the prescribed tolerances. In a few stressed cases, such as `case2746wp_k` and `case3375wp_k`, small active-power balance violations are observed at a limited number of buses. These violations are localized and relatively small in magnitude, while voltage magnitudes, generator limits, thermal limits, and angle-difference constraints remain satisfied. Overall, the feasibility results indicate strong consistency between the APF and AC formulations.

d) *Congestion*: For most medium-scale networks, the APF formulation reproduces the same congestion pattern as the classical AC OPF. Exact congestion matching is observed in

TABLE I: Summary of solver performance across benchmark cases with feasibility and congestion diagnostics

Case	Time	Opt.	Feasibility Check with Constraint Violations (Tolerance)																		Congestion	Max					
			Spd.		Gap		Bus Bal. P (e-1)				Bus Bal. Q (e-1)				V (e-4)	p <sup>g</sup> (e-2)	q <sup>g</sup> (e-2)	θ <sub>i</sub> - θ <sub>j</sub> (e-3)	S <sub>ij</sub> (e-2)	AC	APF	Mis	θ <sub>i</sub> - θ <sub>j</sub>				
			#		Max		Avg		#		Max		Avg		#		Max		Avg		#		#		(deg)		
Small-Scale Systems (9–300 buses)																											
case9	45	0.0000	✓	5e-5	1e-5	✓	1e-5	3e-6	✓	1e-8	4e-9	✓	0	0	✓	0	0	✓	0	0	0	0	0	0	5.5		
case12da	22	0.0000	✓	3e-7	9e-8	✓	8e-7	2e-7	✓	0	0	✓	0	0	✓	0	0	✓	0	0	✓	0	0	0	0.3		
case18	16	0.0000	✓	6e-7	7e-8	✓	2e-7	4e-8	✓	0	0	✓	0	0	✓	0	0	✓	0	0	✓	0	0	0	4.2		
case22	17	0.0000	✓	1e-7	3e-8	✓	2e-7	5e-8	✓	0	0	✓	0	0	✓	0	0	✓	0	0	✓	0	0	0	0.1		
case24_ieee_rts	38	0.0000	✓	6e-5	8e-6	✓	1e-5	2e-6	✓	1e-8	2e-9	✓	4e-8	1e-8	✓	1e-8	2e-9	✓	0	0	✓	0	0	0	11.6		
case30	11	0.0000	✓	2e-5	2e-6	✓	7e-7	1e-7	✓	1e-8	4e-10	✓	0	0	✓	0	0	✓	0	0	✓	2e-7	4e-9	2	2	0	2.5
case33bw	24	0.0000	✓	3e-7	4e-8	✓	6e-7	6e-8	✓	0	0	✓	0	0	✓	0	0	✓	0	0	✓	0	0	0	0	0.2	
case38si	28	0.0000	✓	3e-6	4e-7	✓	6e-6	5e-7	✓	0	0	✓	0	0	✓	0	0	✓	0	0	✓	0	0	0	0	0.2	
case39	45	0.0000	✓	2e-3	1e-4	✓	2e-4	2e-5	✓	1e-8	1e-9	✓	7e-8	3e-8	✓	3e-8	7e-9	✓	0	0	✓	0	0	0	0	6.7	
case51ga	28	0.0000	✓	7e-7	8e-8	✓	9e-7	1e-7	✓	0	0	✓	0	0	✓	0	0	✓	0	0	✓	0	0	0	0	0.2	
case57	72	0.0000	✓	1e-3	4e-5	✓	2e-4	1e-5	✓	1e-8	2e-10	✓	0	0	✓	1e-8	3e-9	✓	0	0	✓	0	0	0	0	4.9	
case69	31	0.0000	✓	4e-7	2e-8	✓	1e-6	5e-8	✓	0	0	✓	0	0	✓	0	0	✓	0	0	✓	0	0	0	0	0.4	
case74ds	36	0.0000	✓	9e-7	3e-8	✓	1e-6	3e-8	✓	0	0	✓	0	0	✓	0	0	✓	0	0	✓	0	0	0	0	0.02	
case118	47	0.0000	✓	3e-4	1e-5	✓	9e-5	3e-6	✓	1e-8	8e-10	✓	1e-8	3e-9	✓	1e-8	2e-9	✓	0	0	✓	0	0	0	0	10.7	
case141	27	0.0000	✓	2e-6	3e-8	✓	3e-6	5e-8	✓	0	0	✓	0	0	✓	0	0	✓	0	0	✓	0	0	0	0	0.1	
case300	38	0.0000	✓	4e-3	6e-5	✓	4e-4	7e-6	✓	1e-8	1e-9	✓	1e-8	6e-10	✓	4e-8	4e-9	✓	0	0	✓	0	0	0	0	20.7	
Medium-Scale pglib_opf Systems (588–3375 buses)																											
case588_sdet	20	0.0018	✓	4e-2	8e-4	✓	1e-2	1e-4	✓	1e-8	9e-11	✓	1e-7	2e-8	✓	4e-8	2e-9	✓	0	0	✓	2e-3	4e-6	15	15	0	11.0
case1354_pegase	27	0.0001	✓	2e-2	1e-4	✓	1e-3	2e-5	✓	1e-8	3e-10	✓	4e-7	3e-8	✓	4e-8	4e-9	✓	0	0	✓	3e-4	3e-7	15	15	0	13.1
case2383wp_k	50	0.0001	✓	5e-2	5e-5	✓	3e-3	5e-6	✓	1e-8	1e-10	✓	1e-7	1e-8	✓	2e-8	4e-9	✓	0	0	✓	1e-3	4e-7	5	5	0	13.5
case2746wp_k	31	0.0000	1	3e-1	1e-3	✓	2e-2	4e-4	✓	1e-8	7e-11	✓	4e-8	2e-9	✓	0	0	✓	0	0	✓	0	0	0	0	13.9	
case2869_pegase	40	0.0000	✓	4e-2	1e-4	✓	2e-3	1e-5	✓	1e-8	1e-10	✓	4e-7	2e-8	✓	0	0	✓	0	0	✓	9e-5	5e-8	20	20	0	15.0
case3375wp_k	29	0.0015	2	3e-1	5e-4	✓	3e-2	7e-5	✓	1e-8	2e-10	✓	2e-7	1e-8	✓	4e-7	5e-9	✓	0	0	✓	2e-2	3e-5	12	11	1	14.5
Large-Scale pglib_opf Systems (4601–10,480 buses)																											
case4601_goc	48	0.0004	4	4e-1	3e-4	✓	6e-2	5e-5	✓	1e-8	1e-10	✓	1e-7	1e-8	✓	1e-8	1e-9	✓	0	0	✓	0	0	1	1	0	9.6
case5658_epigrids	7	0.0001	✓	8e-2	7e-5	✓	8e-3	7e-6	✓	1e-8	6e-11	✓	1e-7	1e-8	✓	1e-8	2e-9	✓	0	0	✓	0	0	0	0	0	7.9
case7336_epigrids	57	0.0004	5	1e-1	3e-4	✓	4e-2	4e-5	✓	1e-8	1e-10	✓	1e-7	1e-8	✓	3e-8	3e-9	✓	0	0	✓	0	0	2	2	0	23.9
case8387_pegase	61	0.0026	1	1e-1	1e-4	✓	2e-2	2e-5	✓	6e-9	6e-12	✓	1e-6	3e-9	✓	0	0	✓	0	0	✓	1	3e-2	2e-6690	691	1	30.0
case9591_goc	23	0.0000	✓	3e-4	3e-7	✓	2e-5	3e-8	✓	1e-8	2e-11	✓	1e-7	2e-8	✓	4e-8	3e-9	✓	0	0	✓	0	0	0	0	0	19.3
case10480_goc	58	0.0000	✓	4e-4	6e-7	✓	1e-4	3e-7	✓	1e-8	3e-11	✓	1e-7	2e-8	✓	3e-8	3e-9	✓	0	0	✓	6e-5	5e-9	7	7	0	25.7

TABLE II: Variable mismatch between AC OPF and APF OPF across medium- and large-scale pglib\_opf systems

		Mismatch (pu / rad)																							
		Medium-Scale Systems								Large-Scale Systems															
		case588	case1354	case2383	case2746	case2869	case3375	case4601	case5658	case7336	case8387	case9591	case10480	Max	Avg										
$p^g$		3e-2	1e-3	6e-3	5e-5	2e-3	2e-5	4e-8	2e-3	2e-5	1e-1	1e-3	4e-3	3e-5	6e-4	1e-6	2e-2	1e-4	1e-0	2e-3	4e-6	2e-8	1e-3	2e-5	
$q^g$		8e-2	5e-3	4e-4	8e-4	9e-3	2e-4	6e-3	7e-5	4e-3	9e-5	4e-2	1e-3	2e-1	4e-3	3e-2	1e-3	1e-1	2e-3	9e-3	4e-2	1e-3	1e-0	7e-3	
$V$		1e-3	6e-4	4e-4	1e-5	1e-4	3e-5	2e-6	2e-7	3e-5	1e-6	5e-4	6e-5	1e-3	1e-4	5e-5	2e-6	2e-4	9e-6	1e-2	8e-5	4e-8	8e-5	6e-6	
$\theta$		6e-3	2e-3	2e-4	4e-5	3e-4	2e-4	4e-3	2e-3	1e-3	7e-5	8e-3	3e-3	3e-3	3e-3	1e-3	7e-4	4e-3	2e-3	2e-2	4e-4	5e-6	4e-6	6e-6	
$P_{ij}/P_{ji}$		4e-2	2e-3	5e-3	1e-4	9e-3	6e-5	2e-1	2e-3	4e-2	1e-4	1e-1	2e-3	3e-1	6e-4	4e-2	2e-4	9e-2	7e-4	6e-1	7e-4	1e-4	4e-7	1e-2	9e-6
$Q_{ij}/Q_{ji}$		7e-2	2e-3	1e-2	2e-4	8e-3	7e-5	2e-2	4e-4	4e-3	3e-5	3e-2	6e-4	2e-1	5e-4	4e-3	4e-5	2e-2	2e-4	7e-1	1e-3	6e-5	1e-7	4e-1	9e-5

all cases except case3375wp\_k, where a single mismatched congested branch is reported. Despite this minor discrepancy, the overall congestion structure and stress locations in the network remain highly consistent between the two formulations.

e)  $\text{Max } \theta_i - \theta_j$ : Maximum branch-wise voltage angle differences for medium-scale systems typically range between  $11^\circ$  and  $15^\circ$ , as reported in Table I. These values are significantly larger than those in small-scale networks and provide a meaningful test of the APF approximation beyond small-angle regimes. The close agreement in angle behavior, together with the small variable mismatches reported in Table II, demonstrates that the APF kernel accurately captures nonlinear angle interactions in meshed transmission networks.

f) *Variable Mismatch Analysis*: For all cases, mismatches in generator dispatch, voltage magnitudes, voltage angles, and branch power flows remain small. Average mismatches are typically several orders of magnitude lower than the corresponding maximum values, indicating that deviations are limited and localized. Even in more stressed networks, the APF formulation closely tracks the AC OPF solution, confirming

strong variable-level agreement between the two models.

3) *Large Systems (4601–10,480 Buses)*: The large-scale category contains the most challenging benchmark systems, including case4601\_goc, case5658\_epigrids, case7336\_epigrids, case8387\_pegase, case9591\_goc, and case10480\_goc. These networks feature large sizes, dense interconnections, and stronger nonlinear effects. All large-scale experiments are conducted using the CasADi-based implementation.

a) *Speedup*: For large-scale systems, the APF formulation continues to provide noticeable computational benefits compared to the classical AC OPF. As shown in Table I, time speedup values range from relatively modest improvements of about 7% in case5658\_epigrids to more significant gains above 50% in cases such as case7336\_epigrids and case10480\_goc. These results indicate that the APF kernel remains effective in improving numerical conditioning even at very large problem sizes.

b) *Optimality Gap*: Across all large-scale cases, the optimality gap remains very small. For most systems, the gap is either zero or below  $10^{-3}\%$ , as reported in Table I. In

particular, `case9591_goc` and `case10480_goc` exhibit zero optimality gap. This demonstrates that the APF formulation preserves objective accuracy even for networks with more than ten thousand buses.

*c) Feasibility:* Several large-scale networks satisfy all true AC feasibility checks, including `case5658_epigrids`, `case9591_goc`, and `case10480_goc`. In other cases, small active-power balance violations are observed at a limited number of buses, such as in `case4601_goc` and `case7336_epigrids`. The most stressed system, `case8387_pegase`, shows more pronounced feasibility and congestion sensitivity. However, similar behavior is also observed in the classical AC OPF for this case, suggesting that these issues are mainly due to numerical conditioning and solver limitations rather than the APF approximation itself.

*d) Congestion:* For most large-scale networks, the APF formulation reproduces the same congestion pattern as the AC OPF. Exact congestion matching is observed in fully feasible cases and in several stressed cases, including `case4601_goc` and `case7336_epigrids`. A small congestion mismatch is only reported for `case8387_pegase`, where one congested line differs between the two formulations, while the overall congestion structure remains largely consistent.

*e) Max  $\theta_i - \theta_j$ :* Maximum branch-wise voltage angle differences in large-scale systems range from approximately  $8^\circ$  to  $30^\circ$ , with the largest value observed in `case8387_pegase`. These large angle spreads provide a stringent test for the APF approximation well beyond small-angle operating regimes. The close agreement between the AC OPF and APF OPF results confirms that the APF kernel can accurately capture nonlinear angular behavior even in very large and heavily loaded networks.

*f) Variable Mismatch Analysis:* Overall, mismatches in generator dispatch, voltage magnitudes, voltage angles, and branch power flows remain small. Average mismatches are consistently much smaller than the corresponding maximum values, indicating that deviations are limited and localized. Larger mismatches are mainly observed in the most stressed case, `case8387_pegase`, which also exhibits feasibility sensitivity in the AC OPF solution. These results show that, even at extreme scales, the APF formulation closely follows the AC OPF solution at the variable level.

*4) Overall Discussion:* Overall, the APF formulation consistently improves computational performance across all network sizes while maintaining close agreement with the classical AC OPF in terms of objective value, feasibility under true AC evaluation, congestion patterns, and voltage angle behavior. Larger speedups are generally observed for more complex and larger networks, reflecting improved numerical conditioning. Cases with feasibility or congestion sensitivity show similar behavior in both formulations, indicating that these effects arise from solver and network limitations rather than from the APF approximation.

## V. CONCLUSION

This paper presented an approximation of the OPF problem, replacing the classical trigonometric power flow kernel with a first-order fractional all-pass mapping equipped with a pre-rotation of angle differences. The proposed approach is effective in that it preserves the essential physical properties of the exponential kernel—unit magnitude, correct loss behavior, and the symmetry of sine and cosine—while

providing smoother, non-oscillatory Jacobians and Hessians that better suit interior-point solvers. Through comprehensive implementation in both YALMIP+IPOPT and CasADi+IPOPT and extensive testing on IEEE, MATPOWER, and PGLib networks up to 10,480 buses, we demonstrated that the APF OPF maintains negligible optimality gaps, reproduces voltage and angle profiles and congestion patterns of the classical model, and reduces IPOPT iterations and computation time, achieving speedups. These results confirm that the proposed APF OPF formulation offers a physics-preserving and solver-friendly alternative to AC OPF.

## REFERENCES

- [1] S. Frank and S. Rebennack, "An introduction to optimal power flow: Theory, formulation, and examples," *IEEE transactions*, vol. 48, no. 12, pp. 1172–1197, 2016.
- [2] S. H. Low, "Convex relaxation of optimal power flow—part i: Formulations and equivalence," *IEEE Transactions on Control of Network Systems*, vol. 1, no. 1, pp. 15–27, 2014.
- [3] D. K. Molzahn, I. A. Hiskens *et al.*, "A survey of relaxations and approximations of the power flow equations," *Foundations and Trends® in Electric Energy Systems*, vol. 4, no. 1-2, pp. 1–221, 2019.
- [4] D. Bienstock and A. Verma, "Strong NP-hardness of AC power flows feasibility," *Operations Research Letters*, vol. 47, no. 6, pp. 494–501, 2019.
- [5] M. Hasanzadeh and A. Kargarian, "ADMM enhancement techniques for distributed optimal power flow," *IEEE Transactions on Power Systems*, 2025.
- [6] R. Madani, S. Sojoudi, and J. Lavaei, "Convex relaxation for optimal power flow problem: Mesh networks," *IEEE Transactions on Power Systems*, vol. 30, no. 1, pp. 199–211, 2014.
- [7] S. Bose, S. H. Low, T. Teeraratkul, and B. Hassibi, "Equivalent relaxations of optimal power flow," *IEEE Transactions on Automatic Control*, vol. 60, no. 3, pp. 729–742, 2014.
- [8] C. Coffrin, H. L. Hijazi, and P. Van Hentenryck, "Strengthening convex relaxations with bound tightening for power network optimization," in *International conference on principles and practice of constraint programming*. Springer, 2015, pp. 39–57.
- [9] R. A. Jabr, "Radial distribution load flow using conic programming," *IEEE transactions on power systems*, vol. 21, no. 3, pp. 1458–1459, 2006.
- [10] P. Buason, S. Misra, J.-P. Watson, and D. K. Molzahn, "Adaptive power flow approximations with second-order sensitivity insights," *IEEE Transactions on Power Systems*, 2024.
- [11] A. Goodwin, J. Maack, and D. Sigler, "Power flow geometry and approximation," *IEEE Transactions on Power Systems*, 2025.
- [12] B. Stott, J. Jardim, and O. Alsaç, "DC power flow revisited," *IEEE Transactions on Power Systems*, vol. 24, no. 3, pp. 1290–1300, 2009.
- [13] J. Lavaei and S. H. Low, "Zero duality gap in optimal power flow problem," *IEEE Transactions on Power systems*, vol. 27, no. 1, pp. 92–107, 2011.
- [14] M. Farivar and S. H. Low, "Branch flow model: Relaxations and convexification—part i," *IEEE Transactions on Power Systems*, vol. 28, no. 3, pp. 2554–2564, 2013.
- [15] A. Wächter and L. T. Biegler, "On the implementation of an interior-point filter line-search algorithm for large-scale nonlinear programming," *Mathematical programming*, vol. 106, no. 1, pp. 25–57, 2006.
- [16] J. Nocedal and S. J. Wright, *Numerical optimization*. Springer, 2006.
- [17] R. D. Zimmerman, C. E. Murillo-Sánchez, and R. J. Thomas, "MATPOWER: Steady-state operations, planning, and analysis tools for power systems research and education," *IEEE Transactions on power systems*, vol. 26, no. 1, pp. 12–19, 2010.
- [18] R. D. Zimmerman and C. E. Murillo-Sánchez, "Matpower 6.0 user's manual," *Power Systems Engineering Research Center*, vol. 9, pp. 65–66, 2016.
- [19] D. P. Bertsekas, "Nonlinear programming," *Journal of the Operational Research Society*, vol. 48, no. 3, pp. 334–334, 1997.
- [20] A. V. Oppenheim, A. S. Willsky, and S. H. Nawab, *Signals & Systems*. Pearson Educación, 1997.
- [21] J. Lofberg, "YALMIP: A toolbox for modeling and optimization in MATLAB," in *2004 IEEE international conference on robotics and automation (IEEE Cat. No. 04CH37508)*. IEEE, 2004, pp. 284–289.
- [22] J. A. Andersson, J. Gillis, G. Horn, J. B. Rawlings, and M. Diehl, "CasADi: a software framework for nonlinear optimization and optimal control," *Mathematical Programming Computation*, vol. 11, no. 1, pp. 1–36, 2019.